Atmos. Chem. Phys. Discuss., 3, 41–73, 2003
www.atmos-chem-phys.org/acpd/3/41/

Atmospheric Chemistry and Physics Discussions

Charging of ice-vapor interfaces

J. Nelson[1] **and M. Baker**[2]

[1]Nelson Scientific, 7-13-8 Oginosato Higashi, Otsu, Shiga 520-0248, Japan
[2]Dept. of Earth and Space Science and Atmospheric Sciences, University of Washington, Seattle, WA 98195-1310, USA

Received: 11 September 2002 – Accepted: 17 December 2002 – Published: 6 January 2003

Correspondence to: J. Nelson (nelson@sd5.so-net.ne.jp)

Abstract

The build-up of intrinsic Bjerrum and ionic defects at ice-vapor interfaces electrically charges ice surfaces and thus gives rise to many phenomena including thermoelectricity, ferroelectric ice films, sparks from objects in blizzards, electromagnetic emissions accompanying cracking in avalanches, glaciers, and sea ice, and charge transfer during ice-ice collisions in thunderstorms. Fletcher's theory of the ice surface in equilibrium proposed that the Bjerrum defects have a higher rate of creation at the surface than in the bulk, which produces a high concentration of surface D^+ defects that attract a high concentration of OH^- ions at the surface. Here, we add to this theory the effect of a moving interface caused by growth or sublimation. This effect can increase the amount of Bjerrum and ionic surface charges more than 10-fold for growth rates near 1 μm s^{-1} and can extend the spatial separation of interior charges in qualitative agreement with many observations. In addition, ice-ice collisions should generate sufficient pressure to melt ice at the contact region and we argue that the ice particle with the initially sharper point at contact loses more mass of melt than the other particle. A simple model of this process with parameters that are consistent with observations leads to predicted collisional charge exchange that semiquantitatively explains the negative charging region of thunderstorms. The model also has implications for snowflake formation, ferroelectric ice, polarization of ice in snowpacks, and chemical reactions in ice surfaces.

1 Introduction

Electrical charging at the ice-vapor interface is revealed directly by surface potentials (Caranti and Illingworth, 1980) and high surface conductivities (Maeno, 1973), and indirectly by processes involving triboelectrification (Petrenko and Colbeck, 1995), ferroelectricity (Iedema et al., 1998), crystal growth (Rydock and Williams, 1991), temperature gradients (Jaccard, 1964), creation of new surfaces (Fifolt et al., 1992), and

electrical attraction of ice crystals to other surfaces (Ohtake and Suchannek, 1970). Such charging can cause ice crystals to orient (Vonnegut, 1965) and possibly levitate (Gibbard et al., 1995) in the electrical atmosphere of thunderclouds, and can modify many atmospheric processes such as collection of ions, aerosols, and droplets (Pruppacher and Klett, 1997) by ice, and aggregation of snow crystals in clouds (Finnegan and Pitter, 1988) and in wind-blown snow (Schmidt, 1982). The transfers of charge when an ice particle strikes another ice surface or another material are examples of contact charging involving electronic insulators, one of the oldest problems of an electrical nature (Castle, 1997). For example, static discharges occur when snow particles recoil from wires and aircraft (Ives, 1938; FAA, 2001). But the most spectacular outcome of the contact charging of ice occurs in thunderstorms when mm-sized ice particles formed from accreted supercooled drops, hereafter graupel, fall at speeds exceeding 5 m s^{-1} and strike small, uplifting ice crystals (Illingworth, 1985). About 20 fC per collision is transferred from one to the other, leading to powerful in-cloud electric fields and often lightning, thus maintaining Earth's electrical circuit. We present a simple model that is consistent with these wide-ranging observations and which allows speculation that the same processes can lead to lightning on Jupiter (Gibbard et al. 1995) and elsewhere in the solar system.

2 Physical basis and approach

Jaccard (1964) developed a microscopic theory of the electrical properties of ice that uses the conservation equations for ions OH^- and H_3O^+ and Bjerrum D and L defects to explain ice thermoelectricity with and without impurities. D and L defects are the majority charge carriers in bulk ice and are responsible for the fact that ice's static dielectric constant exceeds 100 below 0° C. Unlike the ions, the Bjerrum defects create internal electric fields via their polarization of the ice lattice as they migrate such that the D defect effectively has a positive charge and L is negative (Fig. 1). Hereafter we call them D^+ and L^-. Because D^+ and L^- charges arise from rotations of H_2O

molecules that violate the ice rules, they are not free charges and cannot be transferred in collisions. However, because their bulk concentrations are about 10^5 times those of the water ions at equilibrium (Petrenko and Whitworth, 1999; hereafter PW, p. 154), they greatly influence the electric field inside ice. Furthermore, experimental evidence suggests that the Bjerrum defects are important for ice surface charging: collisional charge exchange, presumably due to OH^-, increases with ice crystal growth rate even though surface potential measurements, which detect the neutralization between the OH^- and D^+, have little dependence on growth rate (Caranti and Illingworth, 1980).

Our model is built on the fundamental physical ideas of Jaccard theory but is not sensitive to the molecular structure of Bjerrum defects; we require only their effective charges and mobilities that have been inferred from numerous experiments summarized in PW (p. 154). Because the ice-vapor interface has anomalous structural and electrical properties, Jaccard's model must be supplemented with a description of the surface. The oft-used surface disorder theory in Fletcher (1968) predicts that the surface region has a low activation energy for the creation of D^+ and L^-. The build-up of these defects by their faster creation at the surface and the subsequent drift of L^- to the bulk sets up an electric field that pulls OH^- ions to the surface. For example, recent estimates (Petrenko and Ryzhkin, 1997; hereafter PR) suggest that the equilibrium surface has $\sim 10^6$ and 10^{11} times the bulk concentrations of Bjerrum and ionic defects, respectively.

Many attempts have been made to explain the charging of ice during growth and the subsequent contact charging during collisions. Several of these invoke the fact that the H_3O^+ ion is much more mobile than OH^- in ice (Jaccard, Petrenko and Whitworth), so that charge separation occurs when the ions move down concentration or field gradients at different rates. But we focus here on two new aspects to this problem. One is a "sweeping" effect caused by the moving ice surface when ice grows or sublimates (an example of the classic "Stefan" problem), which can increase or decrease the negative surface charge depending on whether growth or sublimation occurs. However, describing the motion of four mutually-interacting defects in the nonuniform, nonequi-

librium environment of the ice surface is complex; thus the problem is very difficult, even with the simplifications used here. The second aspect is the well-known property of ice to melt under pressure: when the corner of an ice crystal strikes another surface, the force of the collision can produce melt that is then pushed to the side, due to the pressure gradient, and onto the graupel. This process transfers charge to the graupel. Because of the complex ice-atmospheric environment in nature and in experiments, it is difficult to quantitatively compare theory to most ice-charging- related studies. Instead, we use the model to explain the more reliable trends that are listed in Tables 1a and 1b. Furthermore, we use measured ice crystal vapor growth rates and reasonable estimates of two collision parameters to show that our model quantitatively agrees with experiments that simulate thunderstorm charging.

3 Surface charging during growth or sublimation

We assume the ionic and Bjerrum carriers are created and recombined in pairs and migrate in the ice. To treat both equilibrium (stationary surface) and nonequilibrium (moving surface), we write the equations in a reference frame moving with the surface at rate v [m s^{-1}], where v is positive, negative, or zero corresponding to growth, sublimation, or equilibrium. Thus, when $v > 0$, even without the defects hopping between lattice sites, the defects have an effective flux [m^{-2} s^{-1}] towards the ice interior; for example, this flux is $vd(x)$ for D^+, where $d(x)$ is the number concentration of D^+. $d(x)$ obeys the following continuity equation with x being the distance from the surface:

$$\partial d/\partial t = F_B - dl/ < l > \tau_B - j_D', \tag{1}$$

where the prime means derivative with respect to x, F_B [m^{-3} s^{-1}] is the creation rate of Bjerrum D^+ and L^- pairs, $l(x)$ is the L^- concentration with bulk average $< l > \approx 3\times10^{21}$ m^{-3} at –20° C (PW, p. 154), and τ_B is the time scale for D^+ and L^- to recombine to reach steady state. The number flux j_D into the crystal here is vd, but in general includes diffusion and drift in an electric field E, as it does for the other three defects.

We solved Eq. (1) plus equations for E, j_D, and the equations for the other 3 defects numerically for cases with defect creation rates at the surface that are 5–100 times the rates in the bulk. Due to numerical instabilities, we have not directly simulated charge profiles with surface concentrations 10^6–10^{11} times those in the bulk (which are inferred from surface conductivities); nevertheless, we found robust trends in the solutions that permit simple analysis. We describe this analysis here and will describe the simulations elsewhere.

Because the mobilities of all four defects are included, the model is consistent with the high dielectric constant of ice; furthermore, the solutions agree well with the thermoelectric effect in pure ice. Thus, this model is consistent with entries 1–2 of Table 1a. As in Fletcher's theory, we assume a low activation energy of D^+ and L^- at the surface, which results in an excess of surface D^+ over L^- that attracts a high concentration of OH^- to the surface (Fig. 2) thus producing a high dc surface conductivity (entry 3, Table 1a). Examination of our numerical results shows that the important physical features of the charge distributions during growth and sublimation are captured by focusing on the majority carriers D^+ and L^-. For simplicity, here we assume D^+ is immobile, which is consistent with the overall evidence indicating that D^+ is much less mobile than the other three defects (PW, p. 154). In steady state, Eq. (1) predicts

$$vd' = F_B - dl/ < l > \tau_B. \tag{2}$$

Thus, creation-recombination balance does not occur during growth. Even when v is very small and thus $d' \approx d_0' < 0$, where subscript 0 denotes equilibrium, the product on the LHS of Eq. (2) can be significant. We assume small nonequilibrium perturbations of d and l are linear in v; e.g. $d(x) = d_0(x) + v\delta d(x)$. To first order in v, Eq. (2) gives the increase of D^+ as

$$v\delta d(x) = -v < l > \tau_B d_0'(x)/l_0(x), \tag{3}$$

where we have dropped the $\delta l(x)$ term. Including this term increases the charging $\delta d(x)$ for reasons described below, but is less than the term above. Physically,

$v\delta d(x) > 0$ at the surface during growth because the advancing surface effectively "sweeps" surface D^+ inward ($d_0'(x) < 0$ at the surface), and thus $d(x)$ must increase until the recombination rate balances this effective flux (Fig. 3). A distinctive and important property of sweeping (i.e. vd, vl) is its action on all parts of a crystal; growth pushes L^- to the crystal center as D^+ builds up near the surface. This large-scale polarization sets up an electric field that pulls more OH^- ions to the surface and pushes H_30^+ ions towards the crystal center (Fig. 2), in accord with entry 4 in Table 1a. The opposite occurs during sublimation.

Numerical solutions of the equations show that the growth-induced perturbation in the ionic field roughly cancels the perturbed Bjerrum electric field. Thus, we assume the excess OH^- migrate to the surface region to cancel the field from $\delta d(x)$. One then obtains the nonequilibrium addition to the surface ion concentration c_{OH} [#ions m^{-2}] by integrating $\delta d(x)$ over the surface region. We assume $l_0(x) =< l >$, so

$$c_{OH} \sim 0.61 v\, \delta_B d_0(0). \tag{4}$$

The factor 0.61 is the ratio of the effective charge on the D^+ to that on the OH^- (PW, p. 154). In general, the ionic surface concentration c_l is the difference of OH^- and H_3O^+ concentrations that arise in equilibrium, which is estimated by fitting to experiments below, plus the additional amount (e.g. Eq. 4) that comes from growth or sublimation. Because the ions have one elementary charge $\pm e$, the surface charge density $\sigma = -e\, c_{OH}$. For simplicity, we assume c_{OH} is strictly two-dimensional. Equation (4) gives an order-of-magnitude estimate of the nonequilibrium surface charge because it assumes the ions simply respond to the electric field from the Bjerrum defects. A more accurate treatment must consider how the ions and L^- diffuse and interact with the electric field, but such a treatment requires numerical methods. It can be shown that the low mobility of OH^- (compared to H_3O^+) also tends to increase surface OH^-, so that Eq. (4) likely underestimates surface OH^-. For example, the estimate below suggests $\tau_l/\tau_B \approx 10^4$, which would increase the OH^- by nearly 10^4 over Eq. (4) if OH^- was completely immobile and had an increase of creation rate at the surface similar to that of D^+. Another consequence of the tendency of Bjerrum and ionic surface charges

to cancel is that it can explain why ionic charging appears to increase with growth rate (Baker et al., 1987; Berdeklis and List, 2001), whereas the surface potential is relatively insensitive to growth and sublimation rates (Caranti and Illingworth, 1980) (entry 6, Table 1a).

We briefly address the role of D^+ mobility and the reason d not l increases at the surface during growth. Mobility can be neglected if the diffusive flux of D^+, $D_D d'(x)$, is much less than the sweeping flux vd. If the region of large D^+ concentration is limited to a region of thickness Δ then justification for our neglect of D^+ diffusion requires that $D_D/v\Delta << 1$. Presently, the diffusion constant of D^+ is poorly known; for example, Petrenko and Whitworth (PW, p. 154) only suggest that it is much less than that of L^- and might depend on an interaction with vacancies. If D_D equals the H_2O self-diffusion constant at -10°C, that is, about $10^{-15}\,m^2\,s^{-1}$, and $\Delta \sim 0.1\,\mu m$, then mobility can be ignored when $|v| >> 0.01\,\mu m\,s^{-1}$, which is generally satisfied for ice crystals in the atmosphere. Although these values of D_D and Δ are very uncertain, it is fairly well established that D^+ is less mobile than L^-; hence, the qualitative results here should be valid even when the mobility of D^+ influences the charging. Finally, consider Eq. (1) when growth first starts; here, $\partial d/\partial t \approx -vd_0' > 0$ at the surface. Similarly, $\partial l/\partial t \approx -vl_0'$, which is negative at the surface because $l_0' > 0$ according to the analysis in PR. Thus, growth causes d to increase at the surface and l to decrease.

To compare predicted and measured surface charging, we estimate numerical values in Eq. (4) based on various measurements. At -10°C, theory (PR) can explain measured ac and dc electrical properties of the surface if $d_0(0) = 3 \times 10^{27}\,m^{-3}$, which we assume is independent of temperature. The recombination time τ_B is unknown and thus is estimated here. An electrostatic model for the recombination of D^+ and L^- yields $\tau_B = 10^{-9}\varepsilon/3\pi\mu_L q_L < l >$, where μ_L is the mobility of L^- with effective charge $q_L = -0.38e$ and ε is the high-frequency dielectric constant. With recommended values $\mu_L = 2 \times 10^{-8}\,m^2\,V^{-1}\,s^{-1}$ at -20°C, $\varepsilon = 3.16$, and activation energies of 0.25 eV (for μ_L) and 0.73 eV (for $< l >$) (PW, p. 154), $\tau_B \approx 4.6 \times 10^{-5}$ s at -20°C and Eq. (4) predicts $c_{OH} = 1.5 \times 10^{16}$, 8.4×10^{16}, and $5.4 \times 10^{17}\,m^{-2}$ for -10, -20, and

-30°C, respectively, for a growth rate of 1 μm s^{-1}. This calculated growth charging exceeds an estimated equilibrium c_{OH} of $\approx 6 \times 10^{15}$ m^{-2} ($10^{-4} - 10^{-3}$ C m^{-2} from PW, p. 238), which explains entry 5 in Table 1a. During sublimation, $v < 0$ and hence d decreases as I increases at the surface, which pulls H_3O^+ to the surface. Because the dc surface conductivity is proportional to mobility times surface concentration, the increased concentration of the highly-mobile H_3O^+ during sublimation should increase the dc surface conductivity as is measured (entry 7, Table 1a). The success of this model at explaining observations in Table 1a lends confidence to its application to the more difficult case of ice-ice collisions.

4 Charge transfer during ice-ice collisions

An obvious manifestation of large-scale charge separation is lightning, which requires net gain or loss of charge during ice-ice collisions (Illingworth, 1985). In well characterized experiments on ice-ice collisional charging, sub-millimeter, freshly- frozen, mono-dispersed ice spheres near equilibrium collided with a larger ice surface, and induction rings tracked the charge on the spheres before and after impact (Gaskell and Illingworth, 1980; hereafter GI). In these experiments, when the target ice is not growing, the charge transfer ΔQ is roughly independent of the temperature and doping of the target but depends on doping in the ice sphere (Illingworth and Caranti, 1985). This independence is inconsistent with surface state theory (e.g. Castle, 1997) that has been successfully applied to the charging of other materials. We argue below that this unusual property of charging during ice-ice collisions, as well as the other observed relations in Table 1b, arise from a primarily one-way transfer of charged melt.

Experiments by Mason and Dash (2000) found that negative charge transfer between contacting ice surfaces is correlated with a mass transfer, and subsequent analysis indicated that the mass is likely melt (Dash et al., 2001). Pressure melting can explain this finding. In particular, the maximum pressure P_{con} [MPa] at the contact area during

elastic rebound of a small ice crystal on a flat ice surface is (Higa et al., 1998)

$$P_{con} = 195(R_{cr}/r_{tp})^{0.6} U^{0.4}, \quad (5)$$

where R_{cr} is the equivalent sphere radius of the smaller crystal, r_{tp} is its radius of curvature at the initial point of contact (Fig. 4), and U[m s^{-1}] is its impinging speed normal to the surface. We fit Kishimoto and Maruyama's (1998) data on the melting pressure of ice P_{melt}[MPa] to

$$P_{melt} = -12.237\,T - 0.1171\,T^2, \quad (6)$$

for temperature T [$^{\circ}$C] between 0 and -24°C. Equating P_{con} and P_{melt} sets a critical speed above which pressure melting can occur in the contact region. Table 2 shows that these critical speeds are much less than the 5 m s^{-1} updrafts in the strong electrical charging regions of thunderstorms, particularly when $r_{tp} << R_{cr}$. Hence, elasticity theory indicates that pressure melting occurs for typical ice-ice collisions in clouds. But collisional forces change dramatically once melt forms, so the theory by itself cannot predict the amount of melt transfer. To estimate this quantity, a cruder approach is used.

Just before contact, the ice surface on one particle will generally differ from that on the other. It can have a different temperature, charge density, and radius of curvature. In some experiments, for example those of Latham and Mason (1961) and Mason and Dash (2000), the two contacting ice surfaces likely had nearly equal radii of curvature. The theories of Latham and Mason (1961) and Dash et al. (2001), respectively, fit these experiments. However, their theories poorly explain other experimental data: charge transfer based only on temperature differences (Latham and Mason's) has been ruled out as the generator of thunderstorm electricity (Illingworth, 1985), and Dash et al.'s mechanism based on different surface charge densities and temperatures between the two surfaces does not explain measured charge transfers between two nongrowing crystals (GI). In contrast, the initial points of contact between colliding atmospheric ice particles should have very different radii of curvature. We argue here that, in most

cases, the estimated direction of mass transfer is dominated by the difference in radii of curvature between the particles.

When contact occurs, the pressure builds up until melt forms. This melt can form on both particles in the contact region; however, the melt that forms in the initially sharper particle has a much stronger horizontal pressure gradient forcing the fluid to the side and thus to the flatter particle (Fig. 4). If a slice of area a and thickness Δx melts and remains at $P_{melt}(T)$, the work to quasistatically push this fluid to the side is $P_{melt}(T)a\Delta x$. There will be local cooling caused by melting and heating due to viscous dissipation and refreezing, but for simplicity, we assume T remains near its original value. The total work to remove the melt from the sharper particle cannot exceed the loss of incident kinetic energy KE due to the collision. Thus, summing over the volume slices of thickness Δx, the total transferred volume $V[\mathrm{m}^3] = \sum a\Delta x$, is

$$V = f1923R_{cr}^3U^2/P_{melt}(T), \quad (7)$$

where the density of ice at -10°C was assumed and f is the fraction of KE used to transfer mass. Dash et al. (2001) predict about 12-fold more melt volume than that in Eq. (7) because they neglect the work to push the melt aside. Because other processes, including some mass flow from flatter to sharper surface, can also remove KE from the collision, f is less than the inelasticity of the collision. Measurements with ice spheres (Higa et al., 1998) impacting normally on a flat ice surface show that the inelasticity increases with decreasing size and is ≈ 0.5 for $R_{cr} = 1.4$ mm. Thus, f could exceed 0.5 for atmospheric ice crystals if no other processes absorb KE, although $f \sim 0.03 - 0.3$ fits the charging measurements described below (which are likely averages over both normal and glancing collisions). We assume that V is bound by the original point's spherical surface and a slice normal to the contact plane (Fig. 4) and thus the original surface charge in this volume transfers and freezes to the flatter ice surface, which, unless otherwise stated, is assumed to be the graupel. When the graupel is significantly warmer than the crystal, the graupel contact point could melt before that in the crystal and possibly reverse the overall direction of charged-mass transfer. Such a reversal of mass transfer might explain the positive graupel charging (Pereyra

et al., 2000) when the graupel surface was above $\sim -7^\circ$C and the crystals were about -10°C, but in another study, this positive charging did not occur, even when the graupel was 5°C warmer than the crystal (Marshall et al., 1978). Due to the complexity and unknown nature of atmospheric ice-ice collisions, our mass transfer mechanism is presently speculative. The main point is the predicted direction of mass transfer. In addition to the pressure-gradient argument that we described above, other factors should also favor mass transfer to the flatter particle. These include shearing off of the sharper point and partial penetration of the sharper point into the flatter surface. Also, the sharper particle is more likely to melt because it might be softer for two reasons: greater frictional heating if it rubs along the flatter surface and because the sharper points are generally on the particle growing rapidly from the vapor. (Melting can arise from electrostatic pressure within charged ice (PR), which implies that the more highly-charged, fast-growing crystal is softer at its corners than the slower-growing crystal.)

4.1 Charge transfer in equilibrium

We first use measured charge transfers for collisions between frozen droplets and relatively flat, nongrowing surfaces (simulated graupel) to fit f and the equilibrium contribution to σ. We then use these best-fit parameters to compare predicted with measured charge transfers during collisions of facetted growing crystals with graupel. For $R_{cr} < 70\,\mu$m, the charge transfer ΔQ [fC] from nongrowing ice spheres to the simulated graupel at -10°C is $\approx -1.6\,U\,(R_{cr}/50)^2$, where U and R_{cr} have units m s^{-1} and μm, respectively (GI). Using V from Eq. (7) and assuming the spherical cap of Fig. 4, the predicted charge transfer is

$$\Delta Q \approx -3.9 \times 10^5\, U\, \sigma_0 (f/P_{melt})^{0.5}\,(R_{cr}/50)^2, \quad (8)$$

where σ_0 [C m^{-2}] is the ionic surface charge density for stationary interfaces (hereafter "equilibrium") and P_{melt}[MPa] is evaluated at the ambient temperature. The fact that ΔQ is proportional to U and not U^2 is due to geometry: over a realistic range of θ, the area A of a spherical cap increases as $2\sqrt{(\pi r_{tp} V)}$ (Fig. 4). As $\Delta Q \propto A$, it follows that

$\Delta Q \propto V^{0.5} \propto U$, which agrees with entry 2 in Table 1b. Further analysis for the case that the curvature at the contact point r_{tp} differs from the radius of the sphere R_{cr} with the same mass as the crystal leads to ΔQ[fC] $\approx 156 U \sigma_0 (f/P_{melt})^{0.5} r_{tp}^{0.5} R_{cr}^{1.5}$. We fix f so that ΔQ fits measurements; e.g. $\sigma_0 f^{0.5} = 4.3 \times 10^{-5}$ C m^{-2} and thus $f = 0.16$ for an estimated equilibrium σ_0 of 10^{-4} C m^{-2} (PW, p. 238). This fit for the -10°C data also agrees well with Buser and Aufdermaur's measurements at -45°C for $R_{cr} = 10\,\mu$m and $U = 10$ m s^{-1}: using $P_{melt} = 380$ MPa, the predicted charge is $\Delta Q_p = -0.32$ fC versus the measured value of -0.3 fC. Thus, Eq. (8), with constant $\sigma f^{0.5}$, can be used over a wide radius and temperature range.

4.2 Charge transfer between ice crystals and graupel

Neither vapor-grown ice crystals nor graupel are spheres. Vapor-grown ice crystals generally have flat, facetted faces separated by sharp edges and corners. In the absence of some presently unknown alignment force, all collisions should involve the corner of one particle striking a relatively flat section of the other particle. The shape at a crystal corner should be approximately spherical and the resolution in ice crystal photographs suggests that $r_{tp} < 10\,\mu$m. Conversely, graupel surfaces grow when drops of diameter typically exceeding $15\,\mu$m impact, flatten, and freeze. Thus, when graupel does not have frost, the graupel likely has the flatter surface in most collisions. However, as there is considerable variation possible in impact orientation and local shape on a graupel surface, significant variation in ΔQ is predicted; this variation should be particularly large when the graupel has frost or fragile rime branches, which agrees with experiment (entry 3, Table 1b).

The charging due to growth (Eq. 4) plus the fitted equilibrium charge (below Eq. 8) results in a charge transfer to the graupel ΔQ[fC] of

$$\Delta Q = -(\mathrm{K_0} + v f^{0.5} \mathrm{K}_v) U r_{tp}^{0.5} R_{cr}^{1.5} P_{melt}^{-0.5}, \quad (9)$$

where $\mathrm{K_0} = 6.71 \times 10^{-3}$ and $\mathrm{K_v} = 1.25 \exp(11366/T[\mathrm{K}] - 44.9)$ are constants arising

from the conversion of units. For convenience, the units for v, U, r_{tp}, R_{cr}, and P_{melt} are μm s^{-1}, m s^{-1}, μm, μm, and MPa, respectively. The temperature dependence of $\mathrm{K_v}$ is from μ_I and $< I >$. In addition, temperature dependences of $\mathrm{K_0}$, other factors in K_v (e.g. d_0), and collisional and environmental parameters in f could modify Eq. (9) but are presently unknown.

Charge transfer data in the literature are usually presented in terms of maximum crystal dimension D. But, because ice crystals change shape during growth, R_{cr} is not proportional to D; rather, for up to 5 min of growth, measurements find $R_{cr}^3 \propto D^{1.7}$ for tabular crystals and $R_{cr}^3 \propto D^{1.03}$ for columnar crystals (Takahashi et al., 1991). Collision experiments (Keith and Saunders, 1990) with vapor-grown crystals impacting a stationary ice target at -25°C and $U = 10 - 50$ m s^{-1} showed that $\Delta Q \propto D^{0.6-0.8}$. With this growth data, Eq. (9) predicts $\Delta Q \propto D^{0.5-0.9}$ (including both columnar and tabular cases), which agrees well with measurement (entry 4 in Table 1b). Furthermore, for reasonable parameter values, Eq. (9) quantitatively agrees with collision experiments under simulated thunderstorm conditions as shown in Fig. 5. The predicted peaks in the charging near -14.4°C are due to the peaks in v and R_{cr} at this temperature (entry 5, Table 1b). Thus, the variation in growth rate dominates the temperature trend, a factor that has not been explicitly realized in previous models of the charge transfer but is consistent with the oft-stated hypothesis from Baker et al. (1987): "The faster-growing particles (by vapor transfer) acquire positive charge". Other trends are apparent. For example, lower temperatures have larger charging mainly because of the decrease in the L^- concentration with temperature. Also, larger radii of curvature r_{tp} at the contact point have greater charging because of the greater surface area (which can explain entry 6 in Table 1b), and a larger collision efficiency f results in more charging because more ice melts. Finally, we mention that previous charging theories have difficulty explaining the positive charging of graupel when the ice crystals are sublimating (Saunders et al., 2001); but such charging follows from Eq. (9) because $v<0$ and $\mathrm{K_v} >> \mathrm{K_0}$ (entry 7, Table 1b).

5 Further implications of charge transfer model for thunderstorm electrification

5.1 Thunderstorms

In thunderstorms, the collision speed U and the colliding ice particles' masses and growth rates all increase, in general, with increasing updraft speeds. Thus, our model can explain why fast updraft speeds and rapid vapor growth v in clouds are needed to produce vigorous electrification in the main (negative) charging zone of thunderstorms. This model applies to collisions between dry surfaces in which one is sharper than the other; thus it explains the negative charging regime ($\Delta Q < 0$) in which the graupel is relatively smooth (Takahashi, 1978), which is $T < -10^{\circ}$C and cloud liquid water contents $\rho_l \sim 0.3 - 3\,\mathrm{g\,m^{-3}}$ (Fig. 6a). Takahashi's complete data set, which is consistent with the later studies of Pereyra et al. (2000) and Takahashi and Miyawaki (2002), successfully models thunderstorms (Helsdon et al., 2001) and shows that the tripolar nature of thunderstorms arises from the boundary in $T - \rho_l$ space between negative and positive graupel charging. Due to the "knobbly" shape of graupel, predicting exact surface conditions is difficult; but estimates in Williams et al. (1991) indicate that the graupel surface 1) has vapor-grown frost due to the relatively low surface temperature at the lowest ρ_l values (regime of mostly positive charging), 2) sublimates due to the relatively high surface temperature on the graupel at middling ρl values (mostly negative charging), and 3) has liquid water at the highest ρl values (positive charging). In the negative regime, some collisions might involve a facet region of the crystal striking a graupel "knob" (Fig. 6b) and thus transferring charged mass to the crystal. But such collisions can also negatively charge the graupel because sublimation charges the graupel surface positively ($v < 0$ in Eq. (9)). At high ρ_l, the graupel's liquid film would greatly soften the collision, and the dry, cooler surface of a rebounding crystal should instead remove charged liquid from the graupel (Fig. 6g). This should produce overall positive charging (Takahashi, 1978; Graciaa et al., 2001), even if most crystals stick to the graupel. Conversely, positive charging at low ρ_l should result if the frost has the sharper point at the collision (Fig. 6d) or if ice breaks off the graupel (Fig. 6f). In the

former case, Eq. (9) would apply with the opposite sign, but fracture, which does occur in the positive regime at low ρ_l, removes much larger amounts of negative charge (Hallett and Saunders, 1979). A maximum amount of charge when a fractured surface is removed from graupel is estimated by multiplying the charge per area in Eq. (4) by the surface area of the fast-growing frost surface (which neglects neutralizing H_3O^+ in the interior of the ice (Fig. 2)). This amount can exceed -10^4 fC. Thus, even if only a small fraction of the collisions result in fracture, the fractured pieces can dominate the average charge transfer. Our model is consistent with the negative charging regime in thunderstorms and suggests a change to positive at higher and lower ρ_l (entry 8, Table 1b). Therefore, the model here describes a plausible mechanism of thunderstorm electrification.

In addition to the noninductive charge transfer described above, charges induced on ice particles by the in-cloud electric field can also be transferred from particle to particle. This ice-ice inductive charge transfer increases the thunderstorm charging rate after the noninductive ice crystal-graupel mechanism establishes a strong field (Helsdon et al., 2001). Previously, researchers have assumed that these induced charges are transferred by conduction during brief, melt-free collisions (e.g. Illingworth and Caranti, 1985). Given the brevity of such a collisional contact and the relative slowness of conduction, this process has been considered weak. However, if the charge is transferred with melt, as argued here, then ice-ice induction can have greater influence on thunderstorm charging. Thus, charge transfer accompanying mass transfer could partly explain why experiments on ice-ice induction with snow crystals (Scott and Levin, 1970) showed larger charge transfers than the standard inductive theory with conduction and also larger charge transfers than experiments with ice spheres (Illingworth and Caranti, 1985). Furthermore, the ice-ice inductive charge transfer should increase with U as it does with noninductive collisional charge transfer (e.g. Eq. 8), not decrease as previous theories assume, because the charge transfer mechanism should be the same for both inductive and noninductive charging.

5.2 Effect of impurities on charge transfer

Real ice generally contains impurities, which can affect ice electrical properties. Buser and Aufdermaur (1977) found that NH_3 added to frozen droplets increased their negative charge transfer to a metal target, whereas HF reversed the sign of the transfer (entry 9, Table 1b) and had a larger effect than NH_3 for equal concentrations. To explain these trends, we assume that NH_3 and HF substitute for an H_2O molecule in the ice lattice and the concentration of these impurities is greater in the ice interior than it is on the surface. (The latter is consistent with the tendency of ice to reject impurities and freezing of an ice shell around the droplet before the interior is completely frozen.) The substitution of NH_3 in ice is thought to release an OH^-, leaving a relatively immobile D^+ and NH_4^+ (PW p. 99). Some of this OH^- should migrate to the surface, which would increase the OH^- concentration at the surface and lead to the observed result. A similar argument holds for NH_4OH, which would explain results of experiments on sand-ice collisions (Jayaratne, 1991). Conversely, the substitution of HF in ice is thought to release an H_3O^+ and an L^-, leaving a relatively immobile F^- (PW p. 98). Some of the H_3O^+ should migrate to the surface, which would increase the H_3O^+ concentration at the surface and lead to the observed result; in addition, migration of L^- to the surface would produce an electric field that can pull more H_3O^+ to the surface (Fig. 1). HCl should have an effect similar to HF but there are as yet no relevant measurements. Measured charging tendencies (Jayaratne, 1991; Jayaratne et al., 1983) with doping of NaCl and $(NH_4)_2SO_4$ are qualitatively consistent with our model if one assumes that these compounds dissociate and separate in ice according to measured trends (e.g. Workman and Reynolds, 1950), but quantitative prediction is difficult.

6 Implications of the model to other geophysical and planetary phenomena

In this section, we speculate on the possible roles played by charge redistribution and pressure-melting-assisted charge transfer in nonthunderstorm phenomena.

6.1 Charging between ice and other materials

Non-sublimating ice charges positively when sand particles rebound from it (Jayaratne, 1991). As sand is much harder than ice, charged-mass transfer is predicted to be from the ice surface to the sand and thus should positively charge the ice in agreement with measurement. Also, in the laboratory, ice spheres impacting metals at $10\,m\,s^{-1}$ deposit net negative charge during rebound, the only exceptions being metals that easily emit electrons from their surface (Buser and Aufdermaur, 1977; Caranti et al., 1985). The hardness of metals allows pressure melting of ice to occur in such collisions (Table 2), and thus the measurements support the present model. However, such charging, which can be a nuisance when crystals strike antennas and aircraft (FAA, 2001) or cause corona and sparks from objects in contact with blowing snow (Ives, 1938), should be greatly alleviated if the metal is coated by a thin layer of soft material such as silicone rubber. For example, Table 2 shows that ice crystals would require supersonic speeds to transfer charge to rubber via pressure melting.

6.2 Heterogeneous chemistry

Uptake of tropospheric gases by liquid drops is often highly dependent on pH; however, the effect of intrinsic ice surface pH on surface chemical reactions has not been studied. Charging during growth should make the ice surface more basic due to the high OH^- concentration. For example, if 20 fC of surface charge is contained in a volume $V \approx 3\,\mu m^3$ (typical of data in Fig. 5), the average pH upon melting would be 9.6. The pH right at the surface would likely be greater than this average.

6.3 Crystal aggregation

Consequences of surface charging and pressure melting during collisions are largely ignored in atmospheric and planetary studies even though both phenomena can significantly influence various phenomena in these fields. For example, maximum snowflake

size increases dramatically for snowfalls above about -10° C with a smaller peak near -12° C. Aggregation of snow crystals into snowflakes should depend on collision stickiness and electrostatic forces between the crystals. Pressure melting should make the surfaces stickier in collisions. Furthermore, because collisions transfer only a fraction of the surface charge, collisions involving the tip of one crystal and the center of another can retain strong electrostatic attraction even after the charged-mass transfer. Thus, the growth charging in this model can partly explain why tip-center attachments of two snow crystals are common (Finnegan and Pitter, 1988). At low temperatures, the electrostatic attraction can be high for fast-growing frost crystals. This attraction likely explains the fragile "yukimarimo" frostballs that form in Antarctica on the snow surface when light winds break rapidly-grown frost crystals that tumble about and clump together (Kameda et al., 1999). Even at low temperatures, growth charging and pressure melting might influence the aggregation of water-frost covered particles in planetary rings (Jurac et al., 1995) and in planetesimal formation.

6.4 Ferroelectric ice grains

Ice grains in snowpacks are often subjected to temperature gradients that allow sublimation on the warmer side of an air gap and growth on the colder side. According to our model, growth polarizes the lattice with an electric field in one direction, whereas sublimation polarizes in the opposite direction (relative to the surface). Thus, such ice grains can partly polarize from the growing to sublimating ends, which means that the ice becomes partly hydrogen-ordered and ferroelectric along the average temperature gradient. Raman spectroscopy and inelastic neutron scattering on ice from Antarctica, which originated as snowpack, showed proton ordering in samples kept below 237 K (Fukazawa et al., 1998). Such ordering has been a mystery because solid ice in the laboratory transforms to the hydrogen-ordered XI phase only below 72 K; but the growth-sublimation of small grains at low temperature might cause such an orientation to freeze into the lattice and remain until the ice is warmed enough for the Bjerrum defects to migrate back to their usual disordered state. Hence, this surface charging

might partly explain the hydrogen ordering in Antarctic ice. Also, the polarity predicted by our model was measured in crystalline ferroelectric ice films grown at 135—140 K (Iedema et al. 1998). The latter study argued that the polarization was caused by growth, as we do here.

7 Conclusions

Explaining the charging of ice in the atmosphere has enormous difficulties because of the complex nature of ice crystal growth, the four types of charge carriers in ice, and because the atmospheric environment includes updrafts, electric fields, water droplets, and various free charges. The nature of the ice surface is itself the source of much debate, and the collisional process will likely be poorly understood for some time. These complexities justify our simplification of the problem, but it means that the present theory will likely evolve as finer experimental and theoretical details become known. Some details, such as the depth distributions of the charges, non-zero mobility of D^+, and second-order terms might reduce the charging predicted at the outermost surface layer, whereas repulsion of charges at the growing surface (and electrical induction before impact) should push (and pull) more charge to the collision points at the corners and thus increase the charging. Also, disorder of the ice-vapor interface, which is predicted to increase with surface charge (PR), allows greater charged-melt transfer than that proposed here. The microscale roughness of graupel during riming should also be determined. Nevertheless, our theory is based on established properties of ice and is the first that is broadly consistent with wide range of observations. It gives semiquantitative agreement with experiments that, when used in a cloud model, successfully simulate thunderstorm charging. When more data on the electrical properties of the ice-melt interface become available, we can apply the theory to melt growth. Finally, other hydrogen-bonded crystals have ionic and Bjerrum defects (Tonkonogov, 1998) and thus might have surface charging similar to that in ice. Examples include many minerals, and NH_3 and H_2S crystals, which are common in the atmosphere of

the outer planets. Asymmetry between their contacting surfaces is important whether or not pressure melting occurs. For example, collisions can fracture sharp crystal corners, which can lead to large-scale charge separation via gravitational sedimentation. Thus, the surface charging of hydrogen-bonded crystals such as ice by the motion of Bjerrum defects could have widespread implications.

Acknowledgement. Ch. Knight of NCAR made numerous suggestions for improvement including the interpretation of yukimarimo formation, C. Saunders of UMIST found several errors in an early version and suggested comparison to measured surface potentials and sublimating ice, and T. Takahashi of Obirin University made several helpful clarifications. MBB is grateful for the support of the Bosack-Kruger Foundation and also for NSF grant ATM-0211247.

References

Baker, B, Baker, M. B., Jayaratne, E. R., Latham, J., and Saunders, C. P. R.: The influence of diffusional growth rates on the charge transfer accompanying rebounding collisions between ice crystals and soft hailstones, Q. J. R. Meteorol. Soc., 113, 1193–1215, 1987.

Berdeklis, P. and List, R.: The ice crystal-graupel collision charging mechanism of thunderstorm electrification, J. Atmos. Sci., 58, 2751–2770, 2001.

Buser, O. and Aufdermaur, A. N.: Electrification by collisions of ice particles on ice or metal targets, in Electrical Processes in the Atmosphere, Eds. H. Dolezalek and R. Reiter, Steinkopf, Darmstadt, Germany, 1977.

Caranti, J. M. and Illingworth, A. J.: Surface potentials of ice and thunderstorm charge separation, Nature, 284, 44–46, 1980.

Caranti, J. M., Illingworth, A. J., and Marsh, S. J.: The Charging of Ice by Differences in Contact Potential, J. Geophys. Res., D 90, 6041–6046, 1985.

Castle, G. S. P.: Contact charging between insulators, J. Electrostatics, 40 and 41, 13–20, 1997.

Dash, J. G., Mason, B. L., and Wettlaufer, J. S.: Theory of collisional charging of ice: Microphysics of thunderstorm electrification, J. Geophys. Res., 106, 20395–20402, 2001.

Dong, Y. and Hallett, J.: Charge Separation by Ice and Water Drops During Growth and Evaporation, J. Geophys. Res., 97, 20361–20371, 1992.

FAA: Aeronautical Information Manual, Sect. 5 (Potential flight hazards), Subsect. 7-5-10 (Precipitation static), http://www.faa.gov/atpubs/aim/Chap7/aim0705.html, 2001.

Fifolt, D. A., Petrenko, V. F., and Schulson, E. M.: Preliminary study of electromagnetic emissions from cracks in ice, Phil. Mag., B 67, 289–299, 1992.

Finnegan, W. G. and Pitter, R. L.: A postulate of electric multipoles in growing ice crystals: their role in the formation of ice crystal aggregates, Atmos. Res., 22, 235–250, 1988.

Fletcher, N. H.: Surface structure of water and ice II: a revised model, Phil. Mag., 18, 1287–1300, 1968.

Fukazawa, H. Mae, S. Ikeda, S., and Whalley, E.: Proton ordering in Antarctic ice observed by Raman and neutron scattering, Chem. Phys. Lett., 294, 554–558, 1998.

Gaskell, W. and Illingworth, A. J.: Charge transfer accompanying individual collisions between ice particles and its role in thunderstorm electrification, Q. J. Roy. Meteorol. Soc., 106, 841–854, 1980.

Gibbard, S., Levy, E. H., and Lunine, J. I.: Generation of lightning in Jupiter's water cloud, Nature, 378, 592–595, 1995.

Graciaa, A., Creux, P., Lachaise, J., and Schechter, R. S.: Charge transfer between colliding hydrometeors: Role of surface tension gradients, J. Geophys. Res., D 106, 7967–7972, 2001.

Hallett, J. and Saunders, C. P. R.: Charge Separation Associated with Secondary Ice Crystal Production, J. Atmos. Sci., 36, 2230–2235, 1979.

Helsdon, J. H., Wojcik, W. A., and Farley, R. D.: An examination of thunderstorm charging mechanisms using a two-dimensional storm electrification model, J. Geophys. Res., 106, 1165–1192, 2001.

Higa, M. Arakawa, M., and Maeno, N.: Size Dependence of Restitution Coefficients of Ice in Relation to Collision Strength, Icarus, 133, 310–320, 1998.

Iedema, M. J., Dresser, M. J., Doering, D. L., Rowland, J. B., Hess, W. P., Tsekouras, A. A., and Cowin, J. P.: Ferroelectricity in Water Ice, J. Phys. Chem., B 102, 9203–9214, 1998.

Illingworth, A. J.: Charge separation in thunderstorms: small scale processes, J. Geophys. Res., 90, 6026–6032, 1985.

Illingworth, A. J. and Caranti, J. M.: Ice Conductivity Restraints on the Inductive Theory of Thunderstorm Electrification, J. Geophys. Res., D 90, 6033–6039, 1985.

Ives, R. L.: Weather Phenomena of the Colorado Rockies, (see pp. 704-5), J. Franklin Inst., 226, 691–755, 1938.

Jaccard, C.: Thermoelectric effects in ice crystals I. Theory of the steady state, Phys. Kondens. Materie ,1, 143–151, 1964.
Jayaratne, E. R.: Charge separation during the impact of sand on ice and its relevance to theories of thunderstorm electrification, Atmos. Res., 26, 407–424, 1991.
Jayaratne, E. R., Saunders, C. P. R., and Hallett, J.: Laboratory studies of the charging of soft-hail during ice crystal interactions, Quart. J. R. Met. Soc., 109, 609–630, 1983.
Jurac, S., Baragiola, R. A., Johnson, R. E., and Sittler, E. C., Jr.: Charging of ice grains by low-energy plasmas: Application to Saturn's E ring, J. Geophys. Res., A 100, 14821–14831, 1995.
Kameda, T., Hoshimi, H., Azuma, N., and Motoyama, H.: Observation of "yukimarimo" on the snow surface of the inland plateau, Antarctica ice sheet, J. Glaciology, 45, 394–396, 1999.
Keith, W. D. and Saunders, C. P. R.: Charging of aircraft: high-velocity collisions, J. Aircraft, 27, 218–222, 1990.
Kishimoto, Y. and Maruyama, M.: Growth of Ice Ih in Water and Measurements of its Melting Curve, Rev. High Pressure Sci. Technol., 7, 1144–1146, 1998.
Latham, J.: The electrification of frost deposits, Quart. J. Roy. Meteorol. Soc., 89, 265–270, 1963.
Latham, J. and Mason, B. J.: Electric charge transfer associated with temperature gradients in ice, Proc. Roy. Soc., A, 260, 523–536, 1961.
Maeno, N.: Measurements of surface and volume conductivities of single ice crystals, in Physics and Chemistry of Ice, ed. E. Whalley, S. J. Jones, and L. W. Gold, Roy. Soc. Canada, Ottawa, 140–145, 1973.
Marshall, B. J. P., Latham, J., and Saunders, C. P. R.: A laboratory study of charge transfer accompanying the collision of ice crystals with a simulated hailstone, Q. J. R. Met. Soc., 104, 163–178, 1978.
Mason, B. L. and Dash, J. G.: Charge and mass transfer in ice-ice collisions: a mechanism for thunderstorm electrification, J. Geophys. Res., 105, 10185–10192, 2000.
Ohtake, T. and Suchannek, R. G.: Electric properties of ice fog crystals, J. Appl. Meteorol., 9, 289–293, 1970.
Pereyra, R. G., Avila, E. E., Castellano, N. E., and Saunders, C. P. R.: A laboratory study of graupel charging, J. Geophys. Res., 105, 20803–20812, 2000.
Petrenko, V. F. and Colbeck, S. C.: Generation of electric fields by ice and snow friction, J. Appl. Phys., 77, 4518–4521, 1995.

Petrenko, V. F. and Ryzhkin, I. A.: Surface States of Charge Carriers and Electrical Properties of the Surface Layer of Ice, J. Phys. Chem. B, 101, 6285–6289, 1997.
Petrenko, V. F. and Whitworth, R. W.: Physics of Ice, Oxford Univ. Press, Oxford, 1999.
Pruppacher, H. R. and Klett, J. D.: Microphysics of Clouds and Precipitation 2nd edn, Kluwer Academic, Norwell, Massachusetts, 1997.
Rydock, J. P. and Williams, E. R.: Charge separation associated with frost growth, Q. J. R. Meteorol. Soc., 117, 409–420, 1991.
Saunders, C. P. R., Peck, S. L., Aguirre Varela, G. G., Avila, E. E., and Castellano, N. E.: A laboratory study of the influence of water vapor and mixing on the charge transfer process during collisions between ice crystals and graupel, Atmos. Res. 58, 187–203, 2001.
Schmidt, R.: Properties of blowing snow, Rev. Geophys. Space Phys., 20, 39–44, 1982.
Scott, W. D. and Levin, Z.: The effect of potential gradient on the charge separation during interactions of snow crystals with an ice sphere, J. Atmos. Sci., 27, 463–473, 1970.
Takahashi, T.: Riming electrification as a charge generation mechanism in thunderstorms, J. Atmos. Sci., 35, 1536–1548, 1978.
Takahashi, T., Endoh, T., Wakahama, G., and Fukuta, N.: Vapor diffusional growth of free-falling snow crystals between −3 and −23°C, J. Meteorol. Soc. Jpn., 69, 15–30, 1991.
Takahashi, T. and Miyawaki, K.: Reexamination of Riming Electrification, J. Atmos. Sci., 59, 1018–1025, 2002.
Tonkonogov, M. P.: Dielectric spectroscopy of hydrogen-bonded crystals, and proton relaxation, Phys.-Uspekhi, 41, 21–48, 1998.
Vonnegut, B.: Orientation of ice crystals in the electric field of a thunderstorm, Weather, 20, 310–312, 1965.
Williams, E. R., Zhang, R., and Rydock, J.: Mixed-phase microphysics and cloud electrification, J. Atmos. Sci., 48, 2195–2203, 1991.
Workman, E. J. and Reynolds, S. E.: Electrical Phenomena Occurring during the Freezing of Dilute Aqueous Solutions and Their Possible Relationship to Thunderstorm Electricity, Phys. Rev., 78, 254–259, 1950.

Table 1. (a) Relevant electrical properties of ice

#	Experimentally established property
1	High static dielectric constant[a].
2	Thermoelectric effect[b].
3	High surface dc conductivity in equilibrium[c].
4	Nonzero field E and interior charge separation Q over entire crystal during growth[d].
5	Both E and Q greater during growth than in equilibrium[e].
6	Surface potential insensitive to vapor growth or sublimation[f].
7	Surface dc conductivity increases during sublimation[c].

[a] = See Petrenko and Whitworth (1999) chapter 4 and references therein.
[b] = Jaccard (1964)
[c] = Maeno (1973)
[d] = Inferred from the frost growth experiments of Rydock and Williams (1991), Dong and Hallett (1992), and Latham (1963). E positive points from surface to crystal center, which would result from $Q > 0$ at surface and $Q < 0$ in interior. These experiments indicate an excess of OH^- at the surface for growing frost and an excess of H^+ at the surface during sublimation.
[e] = Based on Williams et al.'s (1991) interpretation of Latham's (1963) experiments.
[f] = Caranti and Illingworth (1980)

Table 1. (b) Relations of charge transfer to graupel ΔQ from laboratory experiments

#	Observed relation explained by the model
1	ΔQ mostly independent of physical properties of the flatter surface[a].
2	$\Delta Q \propto U$[a].
3	Variable ΔQ under same conditions; $\Delta Q < 0$ even occurs in $\Delta Q > 0$ regime[a].
4	$\Delta Q \propto D^m$ with m=2 for spheres[a], m< 1 for vapor-grown ice[b].
5	ΔQ peaks near $T = -15^\circ$ C for vapor-grown crystals[c].
6	In equilibrium, ΔQ smaller for vapor-grown ice crystals than for spheres[d].
7	$\Delta Q > 0$ when vapor-grown ice crystals are sublimating[e].
8	For $T < -10^\circ$ C, $\Delta Q < 0$ regime for $\rho_l \approx 0.3 - 3\,\mathrm{g\,m^{-3}}$, $\Delta Q > 0$ regime at other ρ_l[c].
9	ΔQ increases for ice doped with NH_3, but reverses sign with HF doping[f].

Based on experiments with ice spheres ($r_{tp} = R_{cr} = D/2$) and vapor-grown ice ($r_{tp} << R_{cr} < D/2$) impacting graupel. D is the maximum crystal dimension, U is the impact speed, and T is the ambient temperature. In 5 and 8, the experimental clouds had cloud liquid water of density ρ_l; in all others, $\rho_l \sim 0$.
[a] = Based on GI (relations 1, 2, 3, 4) and Marshall et al. (1978) (relations 1, 2, 3) for $\Delta Q < 0$ regime and data in Illingworth and Caranti (1985) (relation 1).
[b] = Keith and Saunders (1990)
[c] = Takahashi (1978) (relations 5 and 8) and Berdeklis and List (2001) (relation 5)
[d] = Compare data in GI to reports of almost no charging when only vapor-grown crystals strike graupel (i.e. $\rho_l \approx 0$ so $v = 0$ in Takahashi, 1978 and Baker et al., 1987)
[e] = Saunders et al. (2001)
[f] = Buser and Aufdermaur (1977)

Table 2. Collision speed U [m s^{-1}] above which pressure melting can occur in ice crystal collisions

R_{cr}/r_{tp}	T [°C] collision type	−5	−10	−15	−20	−25
1	ice sphere-graupel	4.9×10^{-2}	2.5×10^{-1}	5.9×10^{-1}	1.0	1.6
10	snow-graupel	1.6×10^{-3}	7.8×10^{-3}	1.9×10^{-2}	3.3×10^{-2}	5.0×10^{-2}
10	snow-snow	2.2×10^{-3}	1.1×10^{-2}	2.6×10^{-2}	4.7×10^{-2}	7.0×10^{-2}
10	snow-metal	3.9×10^{-4}	1.9×10^{-3}	4.6×10^{-3}	8.3×10^{-3}	1.2×10^{-2}
10	snow-rubber	2.4×10^{4}	1.2×10^{5}	2.9×10^{5}	5.2×10^{5}	7.8×10^{5}

Values from Eqs. (5) and (6). Graupel refers to a flat ice surface. The snow-snow collision is for tip-to-center collisions between two ice crystals of the same mass and follows by replacing R_{cr}^3 with 0.5 R_{cr}^3 in Eq. (5). The bottom two rows apply to snow crystals striking large, flat surfaces of the listed material; metal refers to any material with Young's modulus greatly exceeding that of ice (9.33 GPa), and the estimates for rubber assumed a Young's modulus of 1 MPa.

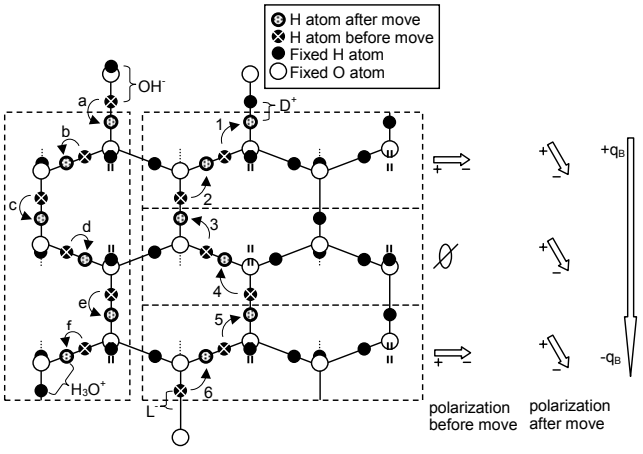

Fig. 1. Creation of a D^+ and L^- defect by the rotation of an H_2O molecule and the subsequent downward migration of the L^- along a prism plane of ice (3 stacked boxes on right). Before step 1, H atoms in the positions of the solid black circles produce net dipole moments that are neither up nor down in all three boxes as shown to the right (e.g. compare H atoms above and below a horizontal line in the middle of a box; the middle box has no dipole moment but the others point to the right). After step 1, the top bond has a D^+ defect (2 H atoms) and the bond below and left has an L^- defect (no H atoms). Step 2 moves an H to the empty bond created by step 1 thus moving the L^- defect down. After 6 such moves, the only L^- is at the bottom, the only D^+ is at the top, and all three boxes now have net polarization pointing down. Thus, the ice effectively has net positive charge on top ($q_B = 0.38e$) and negative charge on bottom; this holds even if, as theory predicts, the 2 H atoms in a D^+ defect are not collinear. Indeed, the middle and lower boxes would be polarized even if the D^+ was not present. Similarly, the vertical box on the left shows the creation of an OH^- and H_3O^+ by the shift of an H-atom along a hydrogen bond (step a) and the subsequent downward migration of H_3O^+ in b–f.

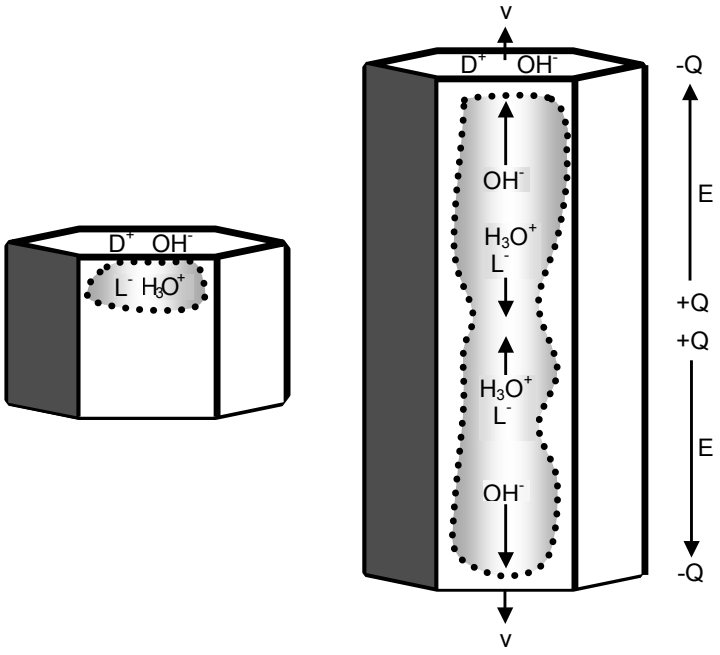

Fig. 2. Regions of concentrated charge without growth or sublimation (left) and during growth at speed v (right). In "equilibrium", the interior L^- and H_3O^+ charges are very near the surface (left; only charges on top surface shown), whereas they build-up near the crystal center during growth (right). Growth also increases surface D^+ and OH^- as described in the text.

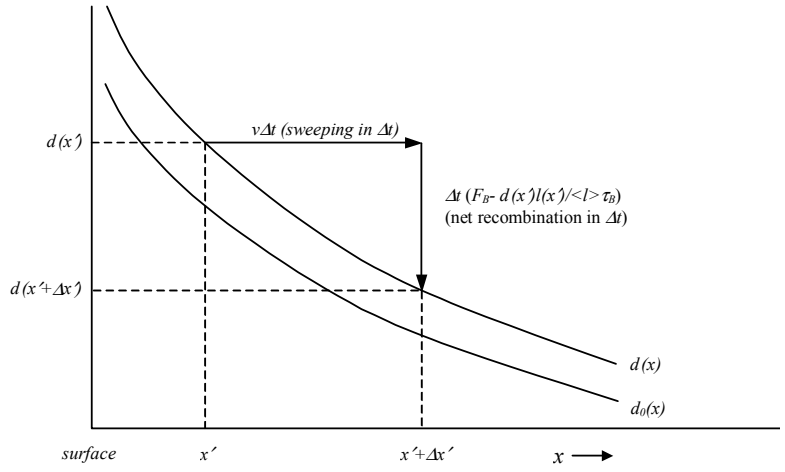

Fig. 3. The balance between the sweeping flux and creation-recombination determines the perturbed D^+ concentration $d(x)$ near the surface. In time Δt growth adds a layer of thickness $v\ \Delta t$, thus effectively sweeping charge $d(x')$ at point x' a distance $\Delta x' = v\Delta t$ from the surface. In this time, net recombination removes an amount $\Delta t\ (F_B - d(x')l(x')/ < l > \tau_B)$.

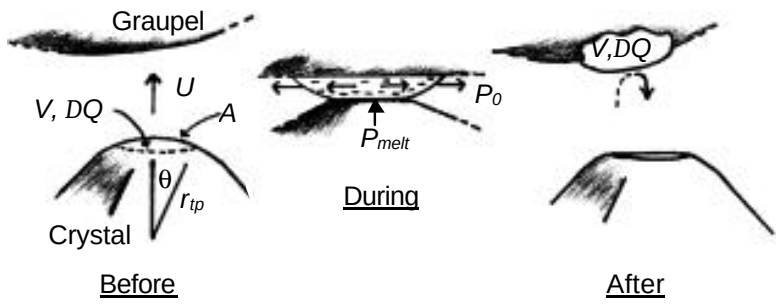

Fig. 4. Mass and charge transfer from the corner of a facetted crystal to the underside of sublimating graupel. The graupel surface is assumed flat over regions of order 15 μm. P_0 ($<<$ P_{melt}) is atmospheric pressure. Before the collision, the initial charge ΔQ at the crystal surface is primarily OH^- if the crystal is growing from the vapor. The collision squeezes this charged mass into melt (exaggerated here) that is pushed outward from a thin region between the ice particles and then freezes onto the graupel. For θ below about 0.61, $A \sim \pi r_{tp}^2 \theta^2$ and $V \sim \pi r_{tp}^3 \theta^4/4$.

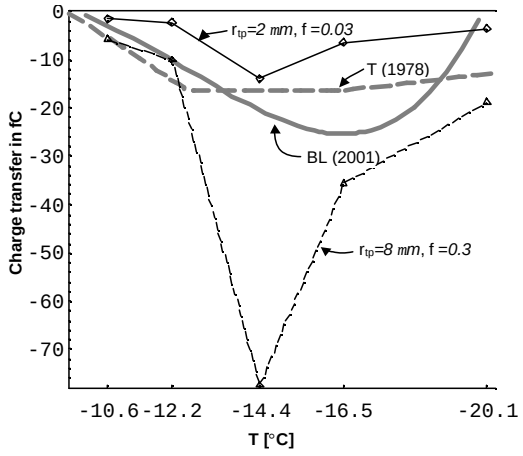

Fig. 5. Comparison of predicted charge transfers ΔQ with experimental data of Takahashi (thick grey, dashed T (1978)) and Berdeklis and List (thick grey, solid BL(2001)) under simulated thunderstorm conditions. Curve T (1978) was made by drawing a line at ρ_l = 1.1 g m^{-3} in Fig. 8 of that reference and linking the resulting contour crossing values by straight lines. BL (2001) is the curve fit to data for conditions under liquid water saturation in Berdeklis and List (2001). Calculations used U = 5.3 m s^{-1}, with measured crystal masses (converted to R_{cr}) and measured growth rates after 3 min of growth from Takahashi et al. (1991). (Measured growth rates were divided by $\sqrt{2}$ because the corners grow slower than the measured points on the crystals.) For the 5 temperatures plotted here, warm to cold, we used growth rates v [μm s^{-1}] and R_{cr} [μm] of (0.12, 35.6), (0.16, 40.6), (0.91, 46.4), (0.31, 45.5), and (0.13, 36.4). Predicted equilibrium charge transfers also peaked near -14.4° C due to the larger R_{cr} at that temperature but were 10–30 times smaller than the growth charge. Melt volume V is from Eq. (7), and area A was computed assuming the melt came from a slice from the sphere as described in Fig. 4; maximum thickness of the transferred mass was $\approx$ 0.5 μm and $\theta < 0.68$, including both cases; thus, Eq. (9) is a good approximation to the calculated values of ΔQ.

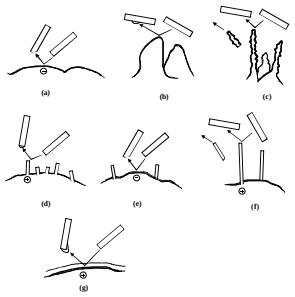

Fig. 6. Mass and charge transfer between vapor-grown crystals, shown as rectangles, and surface regions on graupel, shown at the bottom of each sketch for various graupel surfaces. In a, b, and c, the atmosphere has middling values of liquid water content ρ_l and thus the graupel is sublimating. The flatter graupel surfaces in a and b might result from warmer temperatures, faster droplet collision speeds, or larger droplets freezing to the graupel surface. Case a results in negative charge transfer because the growing crystal transfers mass and negative charge to the graupel. Case b is less clear because the graupel is growing from the melt as the droplets freeze, which might tend to cause build-up of negative ions at the surface, but it is also sublimating, which builds up positive ions at the surface. Case c might occur, but the sign of the charging is hard to predict. d, e, and f occur at low ρ_l when frost, sketched as rectangles, grows on the graupel surface. In d, the negative charge at the corner of the frost transfers to the crystal facet. When the crystal strikes a smooth, frost-free region in e, negative charge transfer occurs just as in case a. Significantly more positive charge is transferred in f because the growing surface is broken off, which carries away all the negative ions at the growing surface. Case g is for sufficiently high ρ_l that the graupel has a layer of liquid water. This case results in positive charging because the outermost surface of the water layer attaches to the crystal and thus drags the negative ions from the water surface to the ice crystal (Takahashi, 1978; Graciaa et al. 2001). These sketches show the great variety of collision possibilities when the crystals are growing from the vapor; also, quantitative charge estimates for cases a, d, e, and f are given in the text. When both ice particles are sublimating, the charging in a and e (and possibly d and f also) should change sign from those shown in the figure.